Doubly Fed Induction Generator for Wind Energy Conversion Systems With Integrated Active Filter Capabilities

N. K. Swami Naidu, *Member, IEEE*, and Bhim Singh, *Fellow, IEEE*

***Abstract*—This paper deals with the operation of doubly fed induction generator (DFIG) with an integrated active filter capabilities using grid-side converter (GSC). The main contribution of this work lies in the control of GSC for supplying harmonics in addition to its slip power transfer. The rotor-side converter (RSC) is used for attaining maximum power extraction and to supply required reactive power to DFIG. This wind energy conversion system (WECS) works as a static compensator (STATCOM) for supplying harmonics even when the wind turbine is in shutdown condition. Control algorithms of both GSC and RSC are presented in detail. The proposed DFIG-based WECS is simulated using MATLAB/Simulink. A prototype of the proposed DFIG-based WECS is developed using a digital signal processor (DSP). Simulated results are validated with test results of the developed DFIG for different practical conditions, such as variable wind speed and unbalanced/single phase loads.**

***Index Terms*—Doubly fed induction generator (DFIG), integrated active filter, nonlinear load, power quality, wind energy conversion system (WECS).**

NOMENCLATURE

v_{ab}, v_{bc}, v_{ca}	Three phase stator voltages.
i_{sa}, i_{sb}, i_{sc}	Three phase stator currents.
i_{ra}, i_{rb}, i_{rc}	Three phase rotor currents.
i_{ga}, i_{gb}, i_{gc}	Three phase grid currents.
i_{la}, i_{lb}, i_{lc}	Three phase load currents.
$i_{\text{gsc}a}, i_{\text{gsc}b}, i_{\text{gsc}c}$	Three phase grid-side convertor (GSC) currents.
i_{dr}	Direct axis rotor current.
i_{qr}	Quadrature axis rotor current.
$\widetilde{i_{ld}}$	Direct axis load current.
$\overline{i_{ld}}$	Direct axis fundamental load current.
P_g	Active power fed to the grid.
Q_g	Reactive power fed to the grid.
P_s	Stator active power.
Q_s	Stator reactive power.
Q_s	Stator reactive power.
P_l	Load active power.
Q_l	Load reactive power.
P_{gsc}	GSC active power.
Q_{gsc}	GSC reactive power.
v_w	Wind speed in m/s.
ω_r	Rotor speed in rad/s.
ω_r^*	Reference rotor speed in rad/s.
θ_e	Angle of grid voltage vector.
θ_r	Electrical rotor angle from encoder.
v_{dc}	DC-link voltage.

Manuscript received August 18, 2014; revised November 18, 2014, March 16, 2015, and May 05, 2015; accepted May 18, 2015. Date of publication June 16, 2015; date of current version July 31, 2015. Paper no. TII-14-0867.

The authors are with the Department of Electrical Engineering, Indian Institute of Technology Delhi, New Delhi 110016, India (e-mail: bsingh@ee.iitd.ac.in; nkswaminaidu@gmail.com).

Color versions of one or more of the figures in this paper are available online at http://ieeexplore.ieee.org.

Digital Object Identifier 10.1109/TII.2015.2446767

I. INTRODUCTION

WITH THE increase in population and industrialization, the energy demand has increased significantly. However, the conventional energy sources such as coal, oil, and gas are limited in nature. Now, there is a need for renewable energy sources for the future energy demand [1]. The other main advantages of this renewable source are eco-friendliness and unlimited in nature [2]. Due to technical advancements, the cost of the wind power produced is comparable to that of conventional power plants. Therefore, the wind energy is the most preferred out of all renewable energy sources [3]. In the initial days, wind turbines have been used as fixed speed wind turbines with squirrel cage induction generator and capacitor banks. Most of the wind turbines are fixed speed because of their simplicity and low cost [4]. By observing wind turbine characteristics, one can clearly identify that for extracting maximum power, the machine should run at varying rotor speeds at different wind speeds. Using modern power electronic converters, the machine is able to run at adjustable speeds [5]. Therefore, these variable speed wind turbines are able to improve the wind energy production [6]. Out of all variable speed wind turbines, doubly fed induction generators (DFIGs) are preferred because of their low cost [7]. The other advantages of this DFIG are the higher energy output, lower converter rating, and better utilization of generators [8]. These DFIGs also provide good damping performance for the weak grid [9]. Independent control of active and reactive power is achieved by the decoupled vector control algorithm presented in [10] and [11]. This vector control of such system is usually realized in synchronously rotating reference frame oriented in either voltage axis or flux axis. In this work, the control of rotor-side converter (RSC) is implemented in voltage-oriented reference frame.

Grid code requirements for the grid connection and operation of wind farms are discussed in [12]. Response of DFIG-based

TABLE I
[35] CURRENT DISTORTION LIMITS FOR GENERAL DISTRIBUTION SYSTEMS IN TERMS OF INDIVIDUAL HARMONICS ORDER (ODD HARMONICS) [35]

I_{sc}/I_L	<11	11 ≤ h ≤17	17 ≤ h ≤ 23	23 ≤ h ≤ 35	35 ≤ h	TDD
< 20	4.0	2.0	1.5	0.6	0.3	5.0
20 < 50	7.0	3.5	2.5	1.0	0.5	8.0
50 < 100	10	4.5	4.0	1.5	0.7	12
100 < 1000	12	5.5	5.0	2.0	1.0	15.0
> 1000	15.0	7.0	6.0	2.5	1.4	20.0

Maximum harmonic current distortion is in percent of I_L.
I_{sc} = maximum short-circuit current at PCC; I_L = maximum demand load current (fundamental frequency component) at PCC.

wind energy conversion system (WECS) to grid disturbance is compared to the fixed speed WECS in [13]. As the wind penetration in the grid becomes significant, the use of variable speed WECS for supplementary jobs such as power smoothening and harmonic mitigation are compulsory in addition to its power generation. This power smoothening is achieved by including super magnetic energy storage systems as proposed in [14]. The other auxiliary services such as reactive power requirement and transient stability limit are achieved by including static compensator (STATCOM) in [15]. A distribution STATCOM (DSTATCOM) coupled with fly-wheel energy storage system is used at the wind farm for mitigating harmonics and frequency disturbances [16]. However, the authors have used two more extra converters for this purpose. A super capacitor energy storage system at the dc link of unified power quality conditioner (UPQC) is proposed in [17] for improving power quality and reliability. In all above methods [15]–[17], the authors have used separate converters for compensating the harmonics and also for controlling the reactive power. However, in later stages, some of the researchers have modified the control algorithms of already existed DFIG converters for mitigating the power quality problems and reactive power compensation [18]–[26]. The harmonics compensation and reactive power control are achieved with the help of existing RSC [18]–[23]. Therefore, harmonics are injected from the RSC into the rotor windings. This creates losses and noise in the machine. These different harmonics in rotating part may also create mechanical unbalance. Moreover, both reactive power compensation and harmonic compensation are achieved in all these methods using RSC control. These methods increase the RSC rating. In [24] and [25], harmonic compensation and reactive power control are done using GSC. Therefore, the harmonics are not passing through machine windings in all these cases. Todeschini and Emanuel [26] have compared three different control algorithms and finally concluded that combined modulation of both RSC and GSC are needed for compensating the harmonics and controlling the reactive power. However, the authors have used direct current control of GSC. Therefore, harmonic compensation is not so effective and total harmonic distortion (THD) is not less than 5% as per IEEE-519 standard given in Table I. The authors have also not verified simulation results experimentally. An indirect current control technique is simple and shows better performance for eliminating harmonics as compared to direct current control [27]–[30].

In this work, a new control algorithm for GSC is proposed for compensating harmonics produced by nonlinear loads using an indirect current control. RSC is used for controlling the reactive power of DFIG. The other main advantage of proposed DFIG is that it works as an active filter even when the wind turbine is in shutdown condition. Therefore, it compensates load reactive power and harmonics at wind turbine stalling case. Both simulation and experimental performances of the proposed integrated active filter-based DFIG are presented in this work. The dynamic performance of the proposed DFIG is also demonstrated for varying wind speeds and changes in unbalanced nonlinear loads at point of common coupling (PCC).

II. SYSTEM CONFIGURATION AND OPERATING PRINCIPLE

Fig. 1 shows a schematic diagram of the proposed DFIG-based WECS with integrated active filter capabilities. In DFIG, the stator is directly connected to the grid as shown in Fig. 1. Two back-to-back connected voltage source converters (VSCs) are placed between the rotor and the grid. Nonlinear loads are connected at PCC as shown in Fig. 1. The proposed DFIG works as an active filter in addition to the active power generation similar to normal DFIG. Harmonics generated by the nonlinear load connected at the PCC distort the PCC voltage. These nonlinear load harmonic currents are mitigated by GSC control, so that the stator and grid currents are harmonic-free. RSC is controlled for achieving maximum power point tracking (MPPT) and also for making unity power factor at the stator side using voltage-oriented reference frame. Synchronous reference frame (SRF) control method is used for extracting the fundamental component of load currents for the GSC control.

III. DESIGN OF DFIG-BASED WECS

Selection of ratings of VSCs and dc-link voltage is very much important for the successful operation of WECS. The ratings of DFIG and dc machine used in this experimental system are given in Appendix. In this section, a detailed design of VSCs and dc-link voltage is discussed for the experimental system used in the laboratory.

A. Selection of DC-Link Voltage

Normally, the dc-link voltage of VSC must be greater than twice the peak of maximum phase voltage. The selection of dc-link voltage depends on both rotor voltage and PCC voltage. While considering from the rotor side, the rotor voltage is slip times the stator voltage. DFIG used in this prototype has stator to rotor turns ratio as 2:1. Normally, the DFIG operating slip is ± 0.3. So, the rotor voltage is always less than the PCC voltage. So, the design criteria for the selection of dc-link voltage can be achieved by considering only PCC voltage. While considering

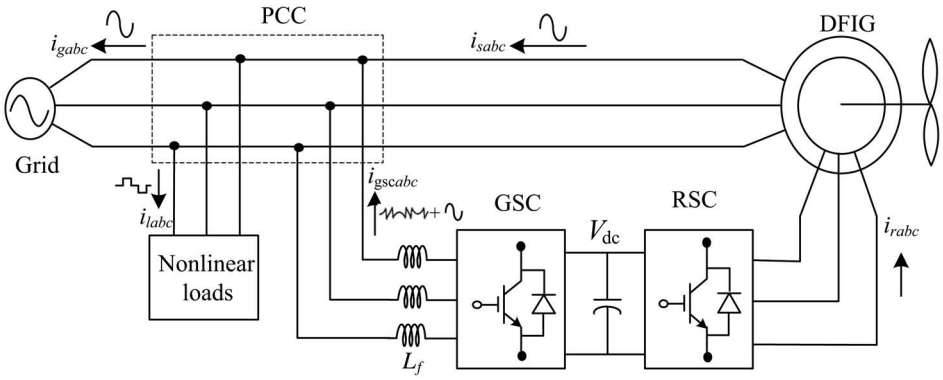

Fig. 1. Proposed system configuration.

from the GSC side, the PCC line voltage (v_{ab}) is 230 V, as the machine is connected in delta mode.

Therefore, the dc-link voltage is estimated as [31]

$$V_{\rm dc} \geq \frac{2\sqrt{2}}{\sqrt{3} * m} V_{ab} \tag{1}$$

where V_{ab} is the line voltage at the PCC. Maximum modulation index is selected as 1 for linear range. The value of dc-link voltage ($V_{\rm dc}$) by (1) is estimated as 375 V. Hence, it is selected as 375 V.

B. Selection of VSC Rating

The DFIG draws a lagging volt-ampere reactive (VAR) for its excitation to build the rated air gap voltage. It is calculated from the machine parameters that the lagging VAR of 2 kVAR is needed when it is running as a motor. In DFIG case, the operating speed range is 0.7 to 1.3 p.u. Therefore, the maximum slip ($s_{\rm max}$) is 0.3. For making unity power factor at the stator side, reactive power of 600 VAR ($S_{\rm max} * Q_{\rm s}$= 0.3 * 2 kVAR) is needed from the rotor side ($Q_{r\rm max}$). The maximum rotor active power is ($S_{\rm max} * P$). The power rating of the DFIG is 5 kW. Therefore, the maximum rotor active power ($P_{r\rm max}$) is 1.5 kW ($0.3 * 5$ kW $= 1.5$ kW). So, the rating of the VSC used as RSC $S_{\rm rated}$ is given as

$$S_{\rm rated} = \sqrt{P_{r\,\rm max}^2 + Q_{r\,\rm max}^2}. \tag{2}$$

Thus, kVA rating of RSC $S_{\rm rated}$ is calculated as 1.615 kVA.

C. Design of Interfacing Inductor

The design of interfacing inductors between GSC and PCC depends upon allowable GSC current limit ($i_{\rm gscpp}$), dc-link voltage, and switching frequency of GSC. Maximum possible GSC line currents are used for the calculation. Maximum line current depends upon the maximum power and the line voltage at GSC. The maximum possible power in the GSC is the slip power. In this case, the slip power is 1.5 kW. Line voltage (V_L) at the GSC is 230 V (the machine is connected in delta mode). So, the line current is obtained as $I_{\rm gsc} = 1.5$ kW/$(\sqrt{3} * 230) = 3.765$ A. Considering the peak ripple current as 25% of rated GSC current, the inductor value is calculated as

$$L_i = \frac{\sqrt{3}\,{\rm mv_{dc}}}{12 a f_m \Delta i_{\rm gsc}} = \frac{\sqrt{3} \times 1 \times 375}{12 \times 1.5 \times 10\,000 \times 0.25 \times 3.76} = 3.8 \text{ mH}. \tag{3}$$

Interfacing inductor between PCC and GSC is selected as 4 mH.

IV. Control Strategy

Control algorithms for both GSC and RSC are presented in this section. Complete control schematic is given in Fig. 2. The control algorithm for emulating wind turbine characteristics using dc machine and Type A chopper is also shown in Fig. 2.

A. Control of RSC

The main purpose of RSC is to extract maximum power with independent control of active and reactive powers. Here, the RSC is controlled in voltage-oriented reference frame. Therefore, the active and reactive powers are controlled by controlling direct and quadrature axis rotor currents ($i_{\rm dr}$ and $i_{\rm qr}$), respectively. Direct axis reference rotor current is selected such that maximum power is extracted for a particular wind speed. This can be achieved by running the DFIG at a rotor speed for a particular wind speed. Therefore, the outer loop is selected as a speed controller for achieving direct axis reference rotor current ($i_{\rm dr}^*$) as

$$i_{\rm dr}^*(k) = i_{\rm dr}^*(k-1) + k_{\rm pd}\{\omega_{\rm er}(k) - \omega_{\rm er}(k-1)\} + k_{\rm id}\omega_{\rm er}(k) \tag{4}$$

where the speed error ($\omega_{\rm er}$) is obtained by subtracting sensed speed (ω_r) from the reference speed (ω_r^*). $k_{\rm pd}$ and $k_{\rm id}$ are the proportional and integral constants of the speed controller. $\omega_{\rm er}(k)$ and $\omega_{\rm er}(k-1)$ are the speed errors at kth and $(k-1)$th instants. $i_{\rm dr}^*(k)$ and $i_{\rm dr}^*(k-1)$ are the direct axis rotor reference current at kth and $(k-1)$th instants. Reference rotor speed (ω_r^*) is estimated by optimal tip speed ratio control for a particular wind speed.

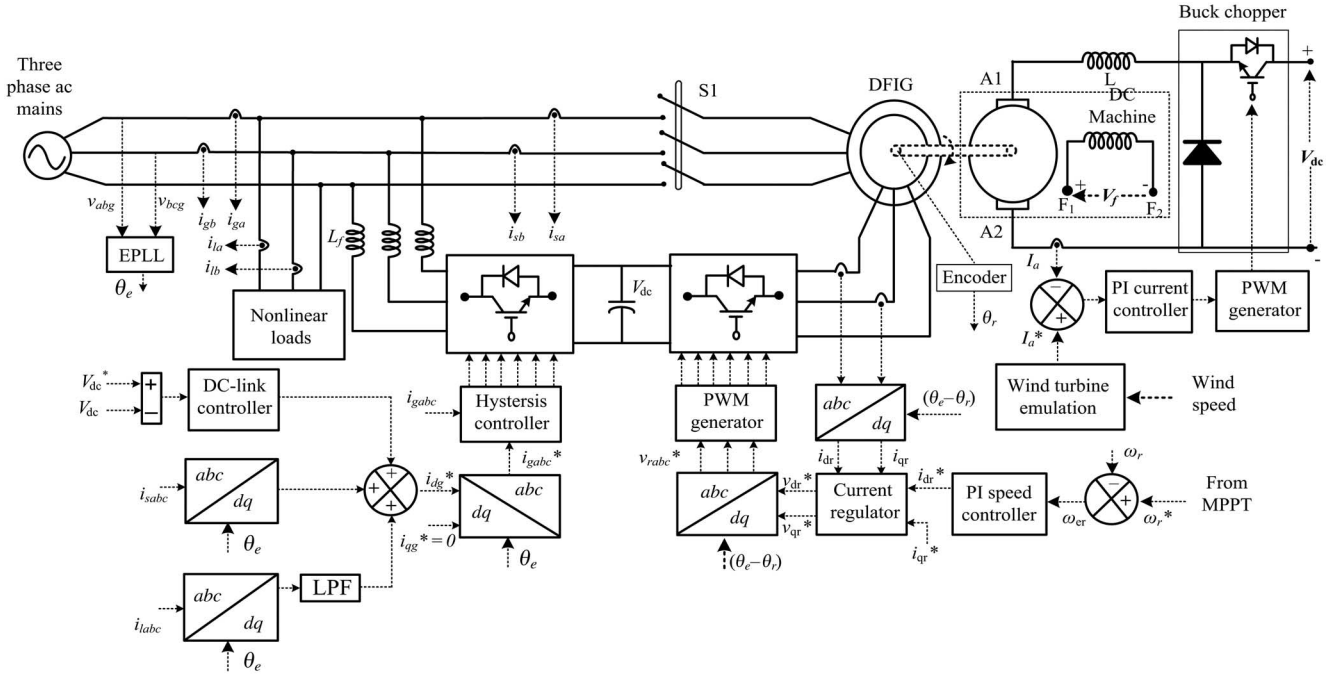

Fig. 2. Control algorithm of the proposed WECS.

The tuning of PI controllers used in both RSC and GSC are achieved using Ziegler Nichols method. Initially, k_{id} value is set to zero and the value of k_{pd} was increased until the response stars oscillating with a period of T_i. Now, the value of k_{pd} is taken as 0.45 k_{pd} and k_{id} is taken as 1.2 k_{pd}/T_i.

Normally, the quadrature axis reference rotor current (i^*_{qr}) is selected such that the stator reactive power (Q_s) is made zero. In this DFIG, quadrature axis reference rotor current (i^*_{qr}) is selected for injecting the required reactive power.

Inner current control loops are taken for control of actual direct and quadrature axis rotor currents (i_{dr} and i_{qr}) close to the direct and quadrature axis reference rotor currents (i^*_{dr} and i^*_{qr}). The rotor currents i_{dr} and i_{qr} are calculated from the sensed rotor currents (i_{ra}, i_{rb}, and i_{rc}) as [32]

$$\text{i}_{\text{dr}} = 2/3 \begin{bmatrix} i_{ra}\ \sin\ \theta_{\text{slip}} + i_{rb} \sin\left(\theta_{\text{slip}} - 2\pi/3\right) \\ +i_{rc}\ \sin\left(\theta_{\text{slip}} + 2\pi/3\right) \end{bmatrix} \tag{5}$$

$$\text{i}_{\text{qr}} = 2/3 \begin{bmatrix} i_{ra} \cos\theta_{\text{slip}} + i_{rb} \cos\left(\theta_{\text{slip}} - 2\pi/3\right) \\ +i_{rc} \cos\left(\theta_{\text{slip}} + 2\pi/3\right) \end{bmatrix} \tag{6}$$

where slip angle (θ_{slip}) is calculated as

$$\theta_{\text{slip}} = \theta_e - \theta_r \tag{7}$$

where θ_e is calculated from PLL for aligning rotor currents into voltage axis. The rotor position (θ_r) is achieved with an encoder.

Direct and quadrature axis rotor voltages (v'_{dr} and v'_{qr}) are obtained from direct and quadrature axis rotor current errors (i_{der} and i_{qer}) as

$$\begin{aligned} v'_{\text{dr}}(k) = v'_{\text{dr}}(k-1) + k_{\text{pdv}}\{i_{\text{der}}(k) - i_{\text{der}}(k-1)\} \\ + k_{\text{idv}} i_{\text{der}}(k) \end{aligned} \tag{8}$$

$$\begin{aligned} v'_{\text{qr}}(k) = v'_{\text{qr}}(k-1) + k_{\text{pqv}}\{i_{\text{qer}}(k) - i_{\text{qer}}(k-1)\} \\ + k_{\text{iqv}} i_{\text{qer}}(k) \end{aligned} \tag{9}$$

where

$$i_{\text{der}} = i^*_{\text{dr}} - i_{\text{dr}} \ \text{ and } \ i_{\text{qer}} = i^*_{\text{qr}} - i_{\text{qr}} \tag{10}$$

where k_{pdv} and k_{idv} are the proportional and integral gains of direct axis current controller. k_{pqv} and k_{iqv} are the proportional and integral gains of quadrature axis current controller.

Direct and quadrature components are decoupled by adding some compensating terms as [26]

$$v^*_{\text{dr}} = v'_{\text{dr}} + (\omega_e - \omega_r)\sigma L_r i_{\text{qr}} \tag{11}$$

$$v^*_{\text{qr}} = v'_{\text{qr}} - (\omega_e - \omega_r)\left(L_m i_{ms} + \sigma L_r i_{\text{dr}}\right). \tag{12}$$

These reference direct and quadrature voltages ($v^*_{\text{dr}}, v^*_{\text{qr}}$) are converted into three phase reference rotor voltages ($v^*_{ra}, v^*_{rb}, v^*_{rc}$) as [32]

$$v^*_{ra} = v^*_{\text{dr}} \sin\theta_{\text{slip}} + v^*_{\text{qr}} \cos\theta_{\text{slip}} \tag{13}$$

$$v^*_{rb} = v^*_{\text{dr}} \sin(\theta_{\text{slip}} - 2\pi/3) + v^*_{\text{qr}} \cos(\theta_{\text{slip}} - 2\pi/3) \tag{14}$$

$$\text{v}^*_{rc} = \text{v}^*_{\text{dr}} \sin(\theta_{\text{slip}} + 2\pi/3) + \ \text{v}^*_{\text{qr}} \cos(\theta_{\text{slip}} + 2\pi/3). \tag{15}$$

These three phase rotor reference voltages (v^*_{ra}, v^*_{rb}, v^*_{rc}) are compared with triangular carrier wave of fixed switching frequency for generating pulse-width modulation (PWM) signals for the RSC.

B. Control of GSC

The novelty of this work lies in the control of this GSC for mitigating the harmonics produced by the nonlinear loads.

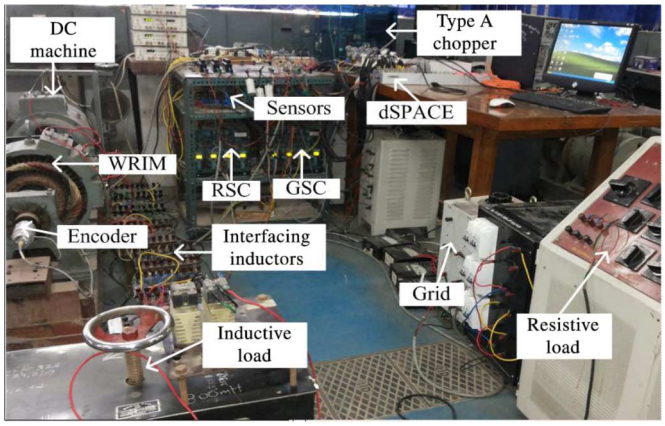

Fig. 3. Photograph of a prototype of DFIG system.

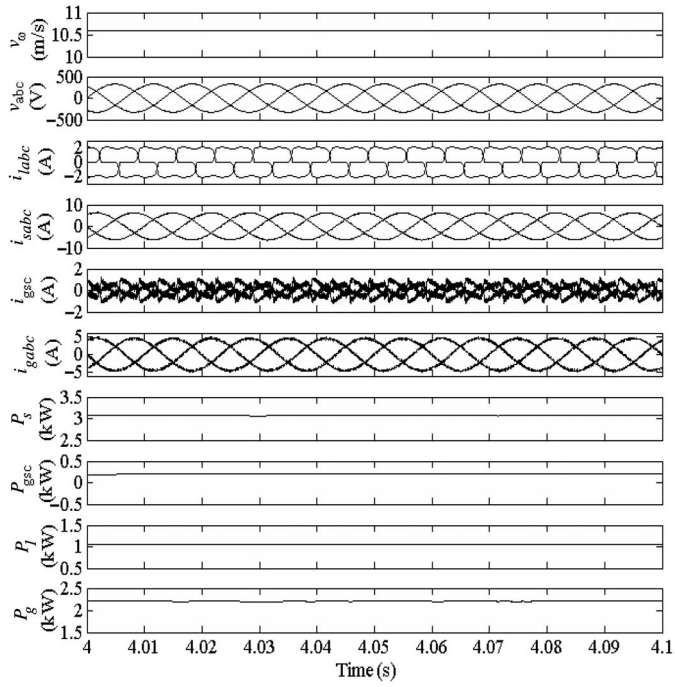

Fig. 4. Simulated performance of the proposed DFIG-based WECS at fixed wind speed of 10.6 m/s (rotor speed of 1750 rpm).

The control block diagram of GSC is shown in Fig. 2. Here, an indirect current control is applied on the grid currents for making them sinusoidal and balanced. Therefore, this GSC supplies the harmonics for making grid currents sinusoidal and balanced. These grid currents are calculated by subtracting the load currents from the summation of stator currents and GSC currents. Active power component of GSC current is obtained by processing the dc-link voltage error ($v_{\rm dce}$) between reference and estimated dc-link voltage ($V_{\rm dc}^*$ and $V_{\rm dc}$) through PI controller as

$$i_{\rm gsc}^*(k) = i_{\rm gsc}^*(k-1) + k_{\rm pdc}\left\{v_{\rm dce}(k) - v_{\rm dce}\,(k-1)\right\} + k_{\rm idc} v_{\rm dce}\,(k) \tag{16}$$

where $k_{\rm pdc}$ and $k_{\rm idc}$ are proportional and integral gains of dc-link voltage controller. $V_{\rm dce}(k)$ and $V_{\rm dce}(k-1)$ are dc-link voltage errors at kth and $(k-1)$th instants. $i_{\rm gsc}^*(k)$ and

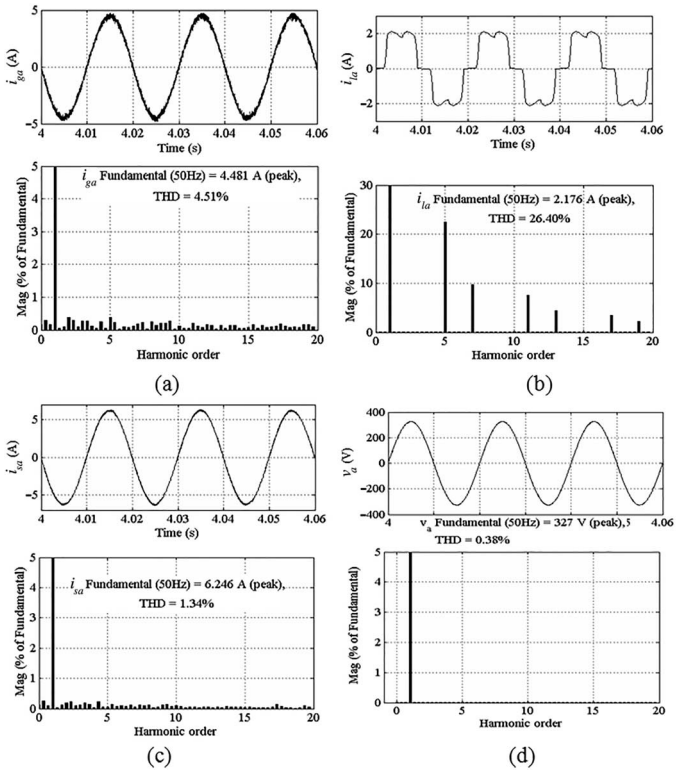

Fig. 5. Simulated waveform and harmonic spectra of (a) grid current (i_{ga}), (b) load current (i_{la}), (c) stator current (i_{sa}), and (d) grid voltage for phase "a" (v_{ga}) at fixed wind speed of 10.6 m/s (rotor speed of 1750 rpm).

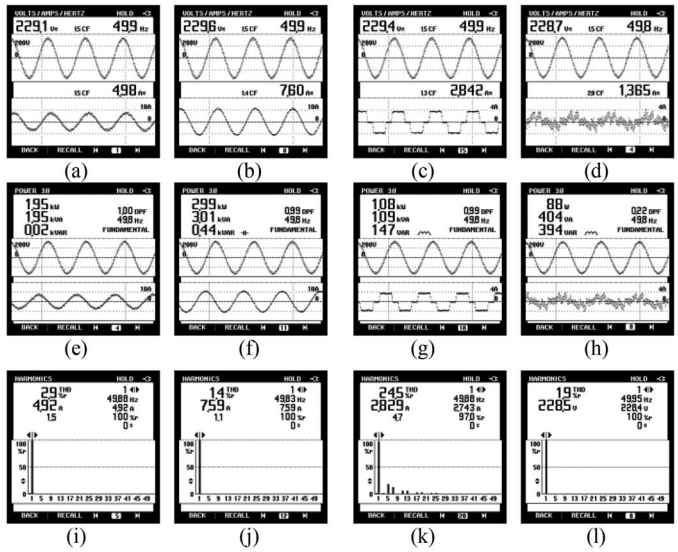

Fig. 6. Performance of the proposed DFIG-based WECS at fixed wind speed of 10.6 m/s (rotor speed of 1750 rpm (a) v_{ab}, i_{ga}; (b) v_{ab}, i_{sa}; (c) v_{ab}, i_{la}; (d) v_{ab}, $i_{\rm gsca}$; (e) P_g; (f) P_s; (g) P_l; (h) $P_{\rm GSC}$; and harmonic spectra of (i) i_{Ga}, (j) i_{sa}, (k) i_{la}, and (l) v_{ab}.

$i_{\rm gsc}^*(k-1)$ are active power component of GSC current at kth and $(k-1)$th instants.

Active power component of stator current (i_{ds}) is obtained from the sensed stator currents (i_{sa}, i_{sb}, and i_{sc}) using *abc* to *dq* transformation as [32]

$$i_{ds} = 2/3\left[i_{sa}\sin\theta_e + i_{sb}\sin(\theta_e - 2\pi/3) + i_{sc}\sin(\theta_e + 2\pi/3)\right]. \tag{17}$$

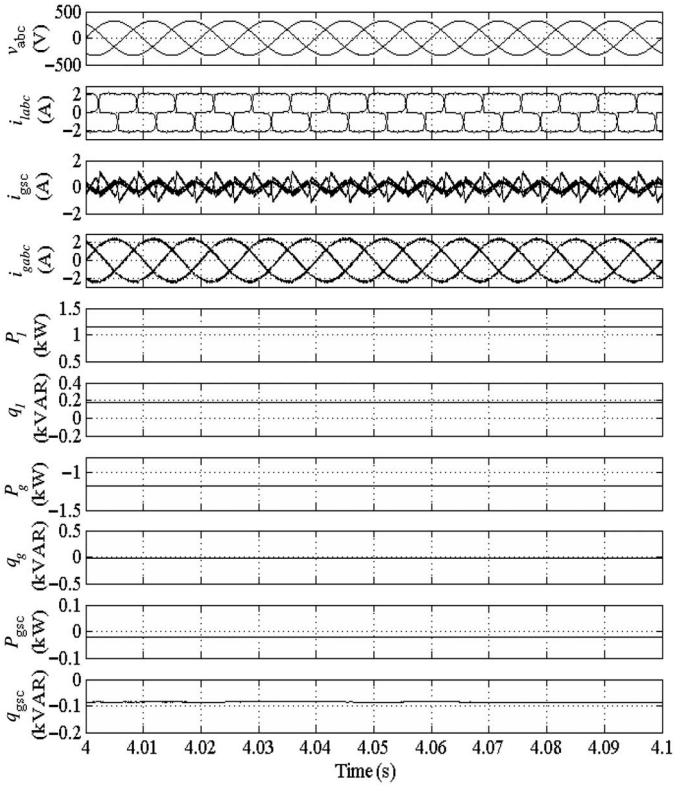

Fig. 7. Simulated performance of the proposed DFIG-based WECS working as a STATCOM at zero wind speed.

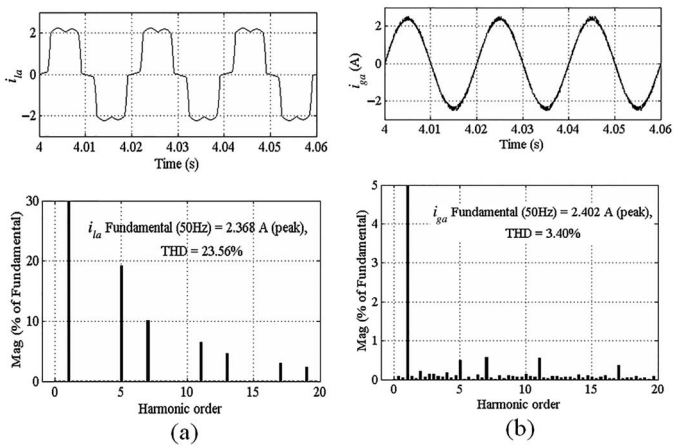

Fig. 8. Simulated waveforms and harmonic spectra of (a) load current (i_{la}) and (b) grid current (i_{ga}) working as a STATCOM at wind turbine shut down condition.

Fundamental active load current ($\overline{i_{ld}}$) is obtained using SRF theory [33]. Instantaneous load currents (i_{labc}) and the value of phase angle from EPLL are used for converting the load currents in to synchronously rotating *dq* frame ($\widetilde{i_{ld}}$). In synchronously rotating frames, fundamental frequency currents are converted into dc quantities and all other harmonics are converted into non-dc quantities with a frequency shift of 50 Hz. DC values of load currents in synchronously rotating *dq* frame ($\overline{i_{ld}}$) are extracted using low-pass filter (LPF).

Direct axis component of reference grid current (i^*_{gd}) is obtained from the direct axis current of stator current (i_{ds}) and

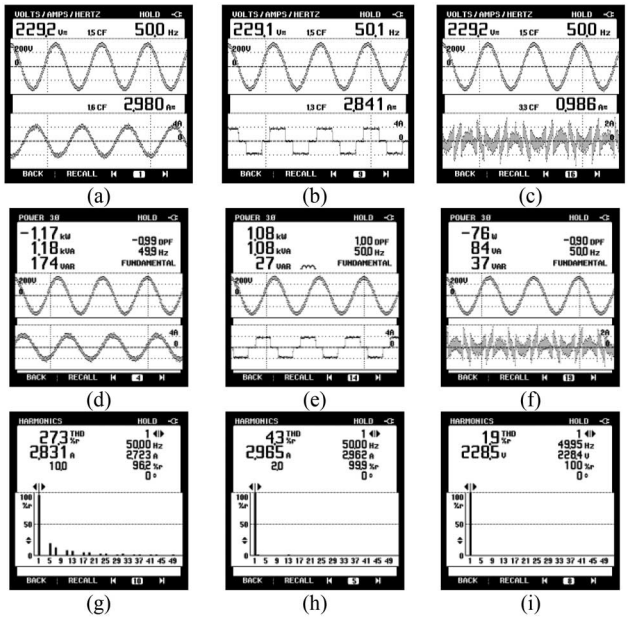

Fig. 9. Performance of the proposed DFIG-based WECS working as a STATCOM at zero wind speed (a) v_{ab}, i_{ga}; (b) v_{ab}, i_{la}; (c) $v_{ab}, i_{\mathrm{gsc}a}$; (d) P_g; (e) P_l; (f) P_{GSC}; and harmonic spectra of (g) i_{la}, (h) i_{ga}, and (i) v_{ab}.

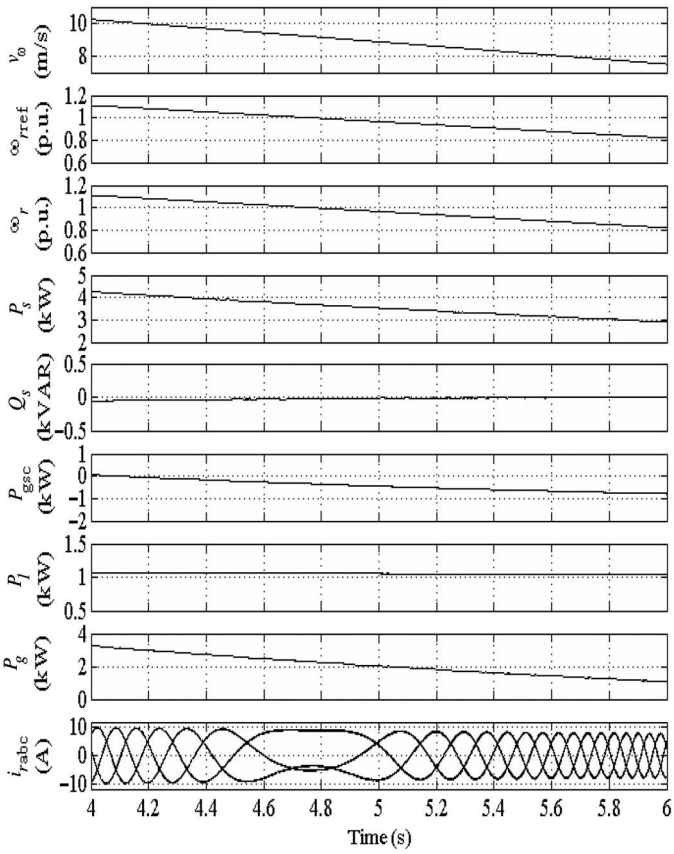

Fig. 10. Simulated performance of proposed DFIG for fall in wind speed.

load current ($\overline{i_{ld}}$) in synchronously rotating frame and the loss component of GSC current (i^*_{gsc}) as

$$\mathrm{i}^*_{gd} = \mathrm{i}^*_{gsc} + i_{ds} - \overline{i_{ld}}. \tag{18}$$

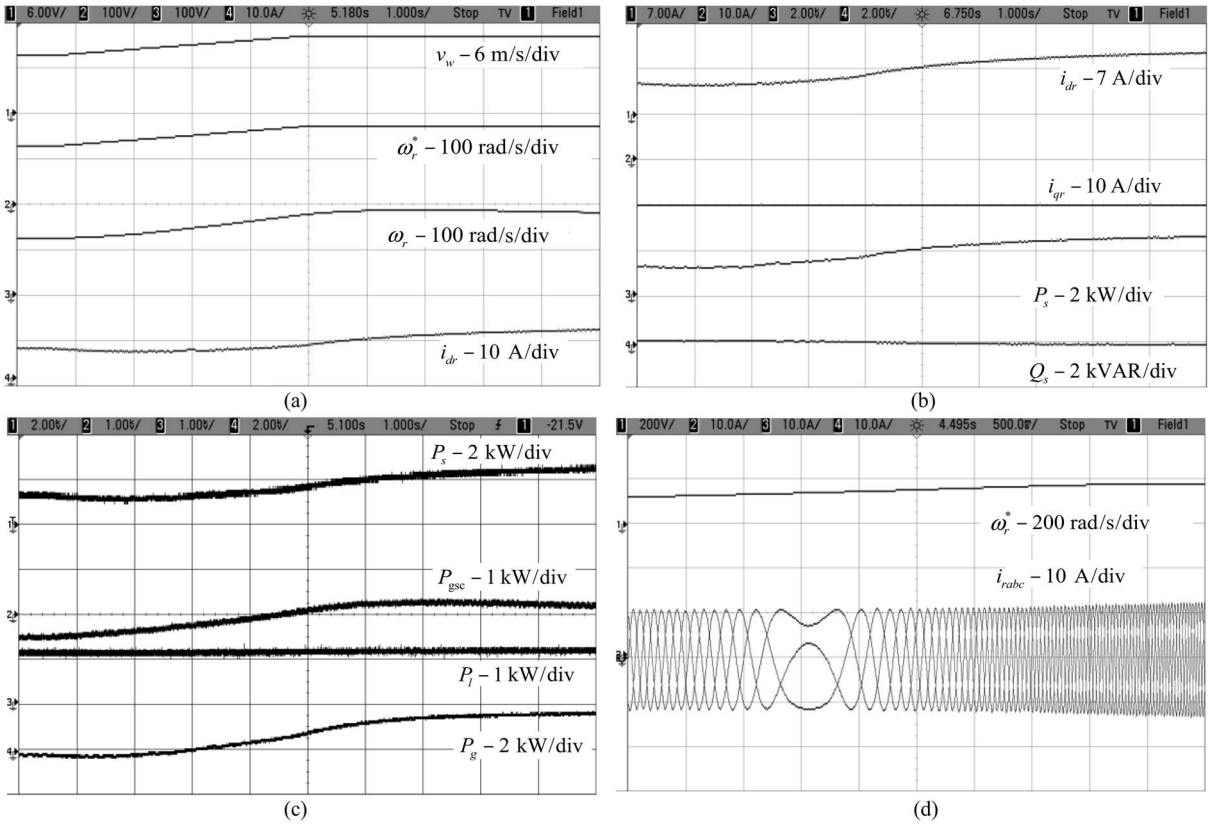

Fig. 11. Dynamic performance of DFIG for the rise in wind speed: (a) v_w, ω_r^*, ω_r, and i_{dr}; (b) i_{dr}, i_{qr} P_s, and Q_s; (c) P_s, P_{gsc}, P_l, and P_g; and (d) ω_r^*, i_{ra}, i_{rb}, and i_{rc}.

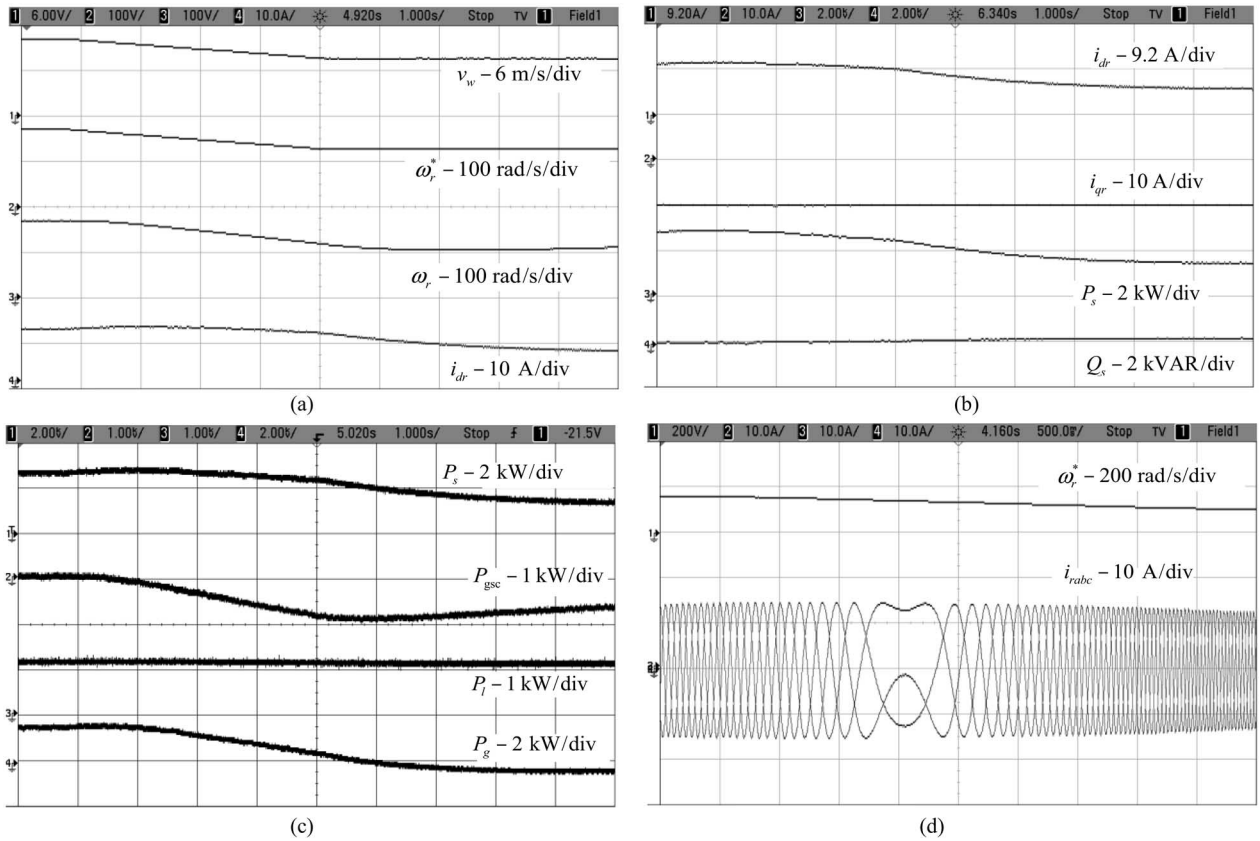

Fig. 12. Dynamic performance of DFIG-based WECS for fall in wind speed: (a) v_w, ω_r^*, ω_r, and i_{dr}; (b) i_{dr}, i_{qr}, P_s, and Q_s; (c) P_s, P_{gsc}, P_l, and P_g; and (d) ω_r^*, i_{ra}, i_{rb}, and i_{rc}.

Quadrature axis component of reference grid current (i^*_{gq}) is selected as zero for not to draw any reactive power from grid.

Reference grid currents (i^*_{ga}, i^*_{gb}, and i^*_{gc}) are calculated from the direct and quadrature axis grid currents (i^*_{gd}, i^*_{gq}) [32]. The hysteresis current controller is used to generate switching pulses for the GSC. The hysteresis controller is a feedback current control where sensed current tracks the reference current within a hysteresis band (i_{hb}) [34]. At every sampling instant, the actual current (i_{gabc}) is compared to the reference current (i^*_{gabc}) as

$$\Delta i_{gabc} = i^*_{gabc} - i_{gabc} \tag{19}$$

$$\text{when } \Delta i_{gabc} > i_{\text{hb}}, \text{ lower switch is turned ON} \tag{20}$$

$$\text{when } \Delta i_{gabc} < -i_{\text{hb}}, \text{ upper switch is turned ON.} \tag{21}$$

Using these equations, gating pulses for three phases of GSC are generated in the same way.

V. Experimental Implementation and Operating Sequence

A prototype of the DFIG-based WECS with integrated active filter capabilities is developed using DSP (dSPACE DS1103) in the laboratory. A photograph of prototype is shown in Fig. 3. In this experimental system, DFIG is coupled with a dc machine. Wind turbine characteristics are emulated using Type A chopper and a dc machine. The dc machine flux is made constant by keeping the field voltage constant. Therefore, the torque of the machine is controlled by controlling the armature current. The torque of the dc machine is selected from the wind turbine characteristics for a particular wind speed and the rotor speed. The armature current is calculated from the demanded torque using flux constant (k_Φ). The duty ratio of the chopper is obtained from the current controller.

Initially, the stator of the DFIG is kept isolated from the grid using switch S1 and the dc machine runs at constant speed by giving fixed duty ratio to the chopper. The GSC is controlled for maintaining the voltage at the dc link. Initially, this GSC works like a simple active filter for supplying the reactive power and harmonics of the local nonlinear loads. Now, this RSC is made ON for making the voltage of the DFIG same as the grid voltage by adjusting the reactive component of rotor current (i_{qr}). An active power component of rotor current (i_{dr}) is made zero for making sure that the stator voltage and the grid voltage are in same phase. Now, the switch S1 is made ON. The control of dc machine is changed from fixed duty ratio mode to wind turbine mode. Still, as there is no active power flow from DFIG to grid, the speed of the machine ramps to maximum depending upon the inertia of the machine. Now, the speed controller is activated. Therefore, the machine speed settles to the reference speed and the active power is fed to the grid.

VI. Results and Discussion

Both simulated and experimental results are presented in this section for validating steady-state and dynamic performances of this proposed DFIG with integrated active filter capabilities.

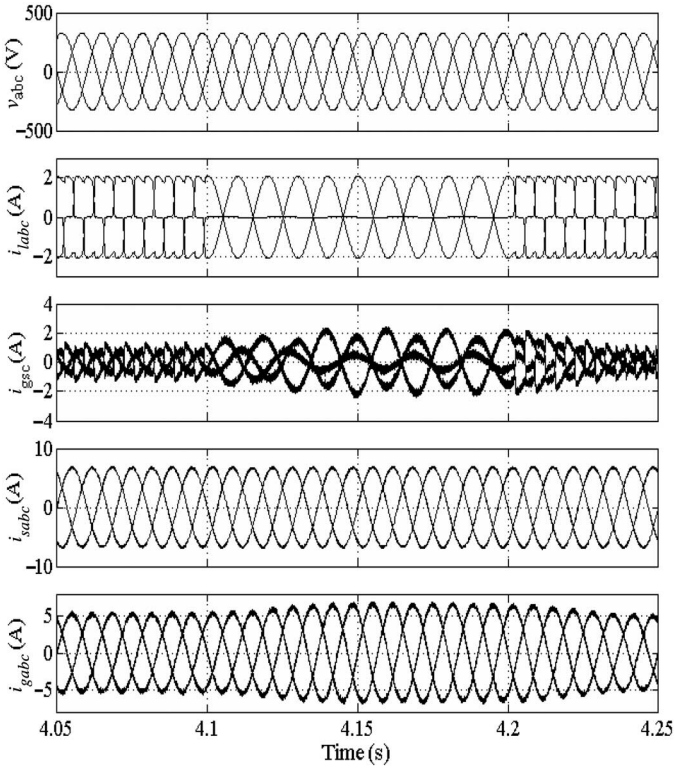

Fig. 13. Dynamic performance of DFIG-based WECS for the sudden removal and application of local loads.

In this section, the working of this proposed GSC is presented as an active filter even when the wind turbine is in shutdown condition. The power that is coming into the PCC through GSC is considered as positive in this paper.

A. Steady-State Performance of DFIG-Based WECS With Integrated Active Filter Capabilities

The simulated performance of this proposed DFIG is presented at a 10.6-m/s wind speed as shown in Fig. 4. As the proposed DFIG is operating at MPPT, the reference speed of the DFIG is selected as 1750 rpm. The load currents are observed to be nonlinear in nature. The GSC is supplying required harmonics currents to the load for making grid currents (i_{gabc}) and stator currents (i_{sabc}) balanced and sinusoidal. Fig. 4 also shows the stator power (P_s), GSC power (P_{gsc}), load power (P_l), and grid power (P_g). At above synchronous speed, the power flow is from the GSC to PCC, so the GSC power is shown as positive. Total power produced by the DFIG is the sum of stator power (P_s) and GSC power (P_{gsc}). After feeding power to the load (P_l), the remaining power is fed to the grid (P_g). Fig. 5 (a)–(d) shows harmonic spectra and waveforms of grid current (i_{ga}), load current (i_{la}), stator current (i_{sa}), and grid voltage (v_{ga}), respectively. From these harmonic spectra, one can understand that grid current and stator current THDs are less than 5% as per IEEE-519 standard [35] limits given in Table I.

Fig. 6 shows test results by performing tests on the developed prototype at a fixed wind speed of 10.6 m/s. These test results are observed similar to the simulated results.

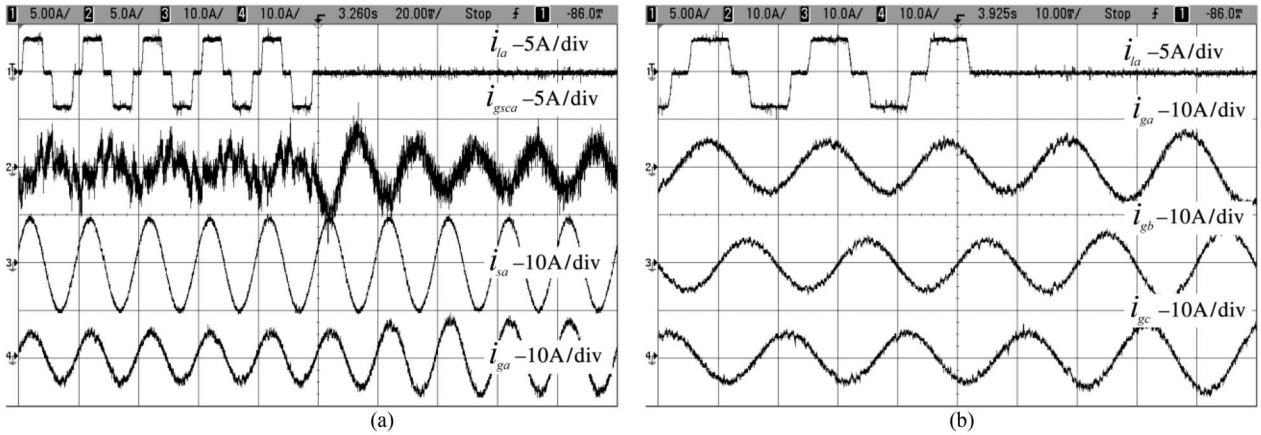

Fig. 14. Dynamic performance of DFIG-based WECS for the sudden removal of one phase of local load. (a) i_{la}, $i_{\mathrm{gsc}a}$, i_{sa}, and i_{ga}. (b) i_{la}, i_{ga},i_{gb}, and i_{gc}.

Fig. 7 shows the simulated results of GSC working as an active filter even when the wind turbine is in stall condition. Here, stator currents are zero, as there is no power production from the DFIG. The load power is supplied from the grid. Therefore, the grid power (P_g) is observed to be negative. Now, this GSC supplies harmonics currents and reactive power. So, the reactive power taken from the grid (Q_g) is observed to be zero. Grid currents are observed to be balanced and sinusoidal even load currents are nonlinear. Fig. 8 shows harmonic spectra of load current and grid current. Even the load current THD is very high, grid current THD is under a limit of IEEE-519 standard.

Fig. 9 shows the test results when GSC is working as an active filter when DFIG is in stall condition. These test results are also observed similar to simulation results. Fig. 9(a)–(c) shows the grid current (i_{ga}), load current (i_{la}), and GSC current ($i_{\mathrm{gsc}a}$) with line voltage (v_{ab}). Grid current (i_{ga}) THD is observed to be less than 5% even in test results.

B. Dynamic Performance of DFIG-Based WECS With Integrated Active Filter Capabilities

Simulated and experimental performances of the proposed DFIG-based WECS are presented for the variation in wind speeds, sudden removal of one phase of local load, and also sudden application of one phase of a local load.

Fig. 10 shows the simulation results for a decrease in wind speed. The reference speed ($\omega_{r\mathrm{ref}}$) is decreased with the decrease in wind speed (v_w) for achieving MPPT operation. The actual rotor speed of the DFIG (ω_r) is also decreased with the reference speed. With the decrease in wind speed, the rotor speed (ω_r) of the DFIG is decreased from supersynchronous speed to the subsynchronous speed and also the slip of the DFIG becomes positive from negative. Therefore, the power flow in the rotor is reversed. Previously, the rotor supplies power through GSC into the grid. As the speed reaches below synchronous speed, the rotor starts taking power from GSC into the rotor. Therefore, the GSC power is becoming negative.

The load power is taken as constant in this case. At high wind speeds, the excess power is feeding to the grid after supplying to the local load. As the wind speed decreases, the power generated by the DFIG is not sufficient to feed local loads. Therefore, the load is supplied from the grid. Therefore, the grid power (P_g) reverses its direction. As the speed changes from supersynchronous speed to the subsynchronous speed, the change in the phase sequence of the rotor currents is observed.

Figs. 11 and 12 show test results for demonstrating the dynamic performance of the proposed DFIG for an increase and decrease in wind speed, respectively. The direct axis component of rotor current (i_{dr}), which is responsible for the generation of active power, needs to be increased with an increase in wind speed for extracting more power. As shown in Fig. 11(b), with an increase in wind speed, the direct axis rotor current (i_{dr}) is increasing, so the stator active power (P_s) is also increasing. From Fig. 11(b), one can clearly observe that quadrature axis rotor current (i_{qr}) is kept constant to keep stator reactive power (Q_s) zero. Therefore, the whole magnetizing current of the DFIG is supplied by the RSC. Hence, the stator is almost maintained at unity power factor by the RSC. Test results in Fig. 12 are observed to be similar to the simulated results.

Fig. 13 shows the simulated performance for demonstrating the load compensation capability of the proposed DFIG. This unbalanced load is emulated by suddenly removing one phase of a load. From the results, one can clearly observe that the stator and grid currents are observed to be balanced and sinusoidal even for the unbalanced load. Fig. 13 shows the dynamic performance of this proposed DFIG-based WECS for the sudden removal and application of load on phase "a." Even for the unbalanced or single phase loads, the stator and grid currents are balanced and sinusoidal by compensating the phase "a" current through GSC. GSC current ($i_{\mathrm{gsc}a}$) in phase "a" is increased suddenly for balancing grid currents. An increase in grid currents (i_{gabc}) is observed as net load decreases with removal of one phase.

Figs. 14 and 15 show the test results of the proposed DFIG for sudden removal and injection of load on phase "a," respectively. Test results are observed to be almost similar to the simulated results.

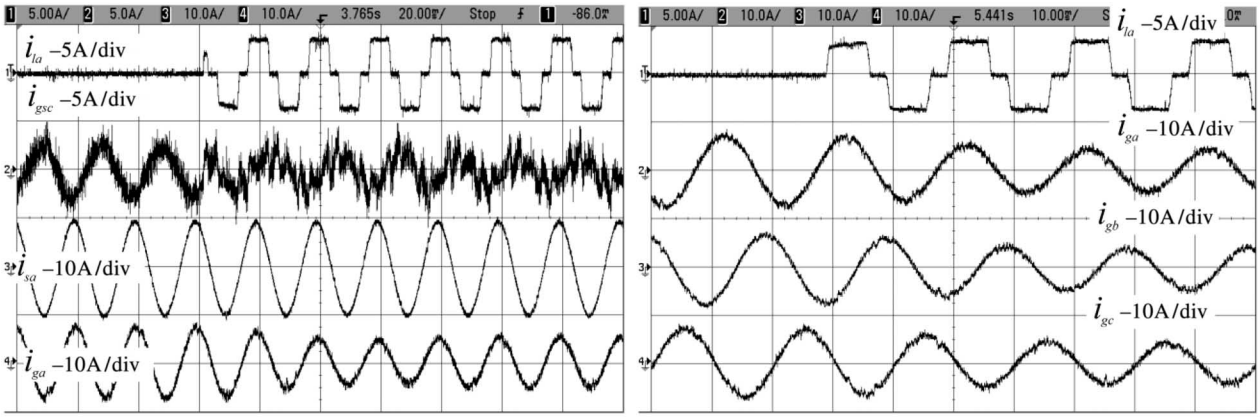

Fig. 15. Dynamic performance of DFIG-based WECS for the sudden injection of one phase of local load. (a) i_{la}, $i_{\mathrm{gsc}a}$, i_{sa}, and i_{ga}. (b) i_{la}, i_{ga}, i_{gb}, and i_{gc}.

VII. Conclusion

The GSC control algorithm of the proposed DFIG has been modified for supplying the harmonics and reactive power of the local loads. In this proposed DFIG, the reactive power for the induction machine has been supplied from the RSC and the load reactive power has been supplied from the GSC. The decoupled control of both active and reactive powers has been achieved by RSC control. The proposed DFIG has also been verified at wind turbine stalling condition for compensating harmonics and reactive power of local loads. This proposed DFIG-based WECS with an integrated active filter has been simulated using MATLAB/Simulink environment, and the simulated results are verified with test results of the developed prototype of this WECS. Steady-state performance of the proposed DFIG has been demonstrated for a wind speed. Dynamic performance of this proposed GSC control algorithm has also been verified for the variation in the wind speeds and for local nonlinear load.

Appendix

1) DFIG: 3.7 kW, R_s= 1.32 ohm, L_{ls} = 6.832 mH, R_2 = 1.708 ohm, L_{lr} = 6.832 mH, R_c = 419.646 ohm, L_m = 0.219 H, $J = 0.1878$ kg · m^2, stator to rotor turns ratio N_r/N_s = 1/2, stator rated rms current = 12 A, rotorrated rms current = 18 A.
2) DC machine: R_a = 1.3 ohms, R_f = 220 ohms, L_a = 7.2 mH, L_f = 7.5 mH, $K_\Phi = 1.3314$.
3) IEEE-519 limits [35]: Current distortion limits for distribution system (120 to 69 000 V) in Table I.
4) Voltage sensors: LEM made LV25P.
5) Current sensors: LEM made LA25P.
6) GSC: IGBT three-leg Semikron inverter module SKM-100GB128DN, $L_f = 4$ mH, 5 kVA star-delta transformer.
7) RSC: IGBT three-leg Semikron inverter module SKM100GB128DN.
8) Controller gains.
   a) Speed controller: $k_{\mathrm{pd}} = 0.1$, $k_{\mathrm{id}} = 0.12$.
   b) Current controller; k_{pdv}, $k_{\mathrm{pqv}} = 100$, k_{idv}, $k_{\mathrm{iqv}} = 130$.
   c) DC-link voltage controller: $k_{\mathrm{pdc}} = 0.08$, $k_{\mathrm{idc}} = 0.02$.

References

[1] D. M. Tagare, *Electric Power Generation the Changing Dimensions*. Piscataway, NJ, USA: IEEE Press, 2011.
[2] G. M. Joselin Herbert, S. Iniyan, and D. Amutha, "A review of technical issues on the development of wind farms," *Renew. Sustain. Energy Rev.*, vol. 32, pp. 619–641, 2014.
[3] I. Munteanu, A. I. Bratcu, N.-A. Cutululis, and E. Ceang, *Optimal Control of Wind Energy Systems Towards a Global Approach*. Berlin, Germany: Springer-Verlag, 2008.
[4] A. A. B. Mohd Zin, H. A. Mahmoud Pesaran, A. B. Khairuddin, L. Jahanshaloo, and O. Shariati, "An overview on doubly fed induction generators controls and contributions to wind based electricity generation," *Renew. Sustain. Energy Rev.*, vol. 27, pp. 692–708, Nov. 2013.
[5] S. S. Murthy, B. Singh, P. K. Goel, and S. K. Tiwari, "A comparative study of fixed speed and variable speed wind energy conversion systems feeding the grid," in *Proc. IEEE Conf. Power Electron. Drive Syst. (PEDS'07)*, Nov. 27–30, 2007, pp. 736–743.
[6] D. S. Zinger and E. Muljadi, "Annualized wind energy improvement using variable speeds," *IEEE Trans. Ind. Appl.*, vol. 33, no. 6, pp. 1444–1447, Nov./Dec. 1997.
[7] H. Polinder, F. F. A. van der Pijl, G. J. de Vilder, and P. J. Tavner, "Comparison of direct-drive and geared generator concepts for wind turbines," *IEEE Trans. Energy Convers.*, vol. 21, no. 3, pp. 725–733, Sep. 2006.
[8] R. Datta and V. T. Ranganathan, "Variable-speed wind power generation using doubly fed wound rotor induction machine—A comparison with alternative schemes," *IEEE Trans. Energy Convers.*, vol. 17, no. 3, pp. 414–421, Sep. 2002.
[9] E. Muljadi, C. P. Butterfield, B. Parsons, and A Ellis, "Effect of variable speed wind turbine generator on stability of a weak grid," *IEEE Trans. Energy Convers.*, vol. 22, no. 1, pp. 29–36, Mar. 2007.
[10] R. Pena, J. C. Clare, and G. M. Asher, "Doubly fed induction generator using back-to-back PWM converters and its application to variable-speed wind-energy generation," *IEE Proc. Elect. Power Appl.*, vol. 143, no. 3, pp. 231–241, May 1996.
[11] S. Muller, M. Deicke, and R. W. De Doncker, "Doubly fed induction generator systems for wind turbines," *IEEE Ind. Appl. Mag.*, vol. 8, no. 3, pp. 26–33, May/Jun. 2002.
[12] W. Qiao and R. G. Harley, "Grid connection requirements and solutions for DFIG wind turbines," in *Proc. IEEE Energy 2030 Conf. (ENERGY'08)*, Nov. 17–18, 2008, pp. 1–8.
[13] A. Petersson, T. Thiringer, L. Harnefors, and T. Petru, "Modeling and experimental verification of grid interaction of a DFIG wind turbine," *IEEE Trans. Energy Convers.*, vol. 20, no. 4, pp. 878–886, Dec. 2005.
[14] H. M. Hasanien, "A set-membership affine projection algorithm-based adaptive-controlled SMES units for wind farms output power smoothing," *IEEE Trans. Sustain. Energy*, vol. 5, no. 4, pp. 1226–1233, Oct. 2014.
[15] Z. Saad-Saoud, M. L. Lisboa, J. B. Ekanayake, N. Jenkins, and G. Strbac, "Application of STATCOMs to wind farms," *IEE Proc. Gener. Transmiss. Distrib.*, vol. 145, no. 5, pp. 511–516, Sep. 1998.
[16] G. O. Suvire and P. E. Mercado, "Combined control of a distribution static synchronous compensator/flywheel energy storage system for wind energy applications," *IET Gener. Transmiss. Distrib.*, vol. 6, no. 6, pp. 483–492, Jun. 2012.

[17] D. Somayajula and M. L. Crow, "An ultra capacitor integrated power conditioner for intermittency smoothing and improving power quality of distribution grid," *IEEE Trans. Sustain. Energy*, vol. 5, no. 4, pp. 1145–1155, Oct. 2014.
[18] M. T. Abolhassani, P. Enjeti, and H. Toliyat, "Integrated doubly fed electric alternator/active filter (IDEA), a viable power quality solution, for wind energy conversion systems," *IEEE Trans. Energy Convers.*, vol. 23, no. 2, pp. 642–650, Jun. 2008.
[19] A. Gaillard, P. Poure, and S. Saadate, "Active filtering capability of WECS with DFIG for grid power quality improvement," in *Proc. IEEE Int. Symp. Ind. Electron.*, Jun. 30, 2008, pp. 2365–2370.
[20] A. Gaillard, P. Poure, and S. Saadate, "Reactive power compensation and active filtering capability of WECS with DFIG without any overrating," *Wind Energy*, vol. 13, pp. 603–614, 2009.
[21] M. Boutoubat, L. Mokrani, and M. Machmoum, "Control of a wind energy conversion system equipped by a DFIG for active power generation and power quality improvement," *Renew. Energy*, vol. 50, pp. 378–386, Feb. 2013.
[22] A. Ejlali and D. Arab Khaburi, "Power quality improvement using nonlinear-load compensation capability of variable speed DFIG based on DPC-SVM method," in *Proc. 5th Power Electron. Drive Syst. Technol. Conf. (PEDSTC)*, Feb. 5–6, 2014, pp. 280–284.
[23] B. Mohamed, L. Mokrani, and M. Machmoum, "Full capability of harmonic current mitigation for a wind energy system," *Elect. Power Comp. Syst.*, vol. 42, no. 15, pp. 1743–1753, 2009.
[24] E. Tremblay, A. Chandra, and P. J. Lagace, "Grid-side converter control of DFIG wind turbines to enhance power quality of distribution network," in *Proc. IEEE PES Gen. Meeting*, 2006, p. 6.
[25] E. Tremblay, S. Atayde, and A Chandra, "Direct power control of a DFIG-based WECS with active filter capabilities," in *Proc. IEEE Elect. Power Energy Conf. (EPEC)*, Oct. 22–23, 2009, pp. 1–6.
[26] G. Todeschini and A. E. Emanuel, "Wind energy conversion system as an active filter: Design and comparison of three control systems," *IET Renew. Power Gener.*, vol. 4, no. 4, pp. 341–353, Jul. 2010.
[27] B. N. Singh, A. Chandra, and K. Al-Haddad, "Performance comparison of two current control techniques applied to an active filter," in *Proc. 8th Int. Conf. Harmonics Qual. Power Proc.*, Oct. 14–18, 1998, vol. 1, pp. 133–138.
[28] B. N. Singh, A. Chandra, and K. Al-Haddad, "DSP-based indirect-current-controlled STATCOM. I. Evaluation of current control techniques," *IEE Proc. Elect. Power Appl.*, vol. 147, no. 2, pp. 107–112, Mar. 2000.
[29] B. N. Singh, A. Chandra, and K. Al-Haddad, "DSP-based indirect-current-controlled STATCOM. II. Multifunctional capabilities," *IEE Proc. Elect. Power Appl.*, vol. 147, no. 2, pp. 113–118, Mar. 2000.
[30] B. N. Singh, B. Singh, A. Chandra, P. Rastgoufard, and K. Al-Haddad, "An improved control algorithm for active filters," *IEEE Trans. Power Del.*, vol. 22, no. 2, pp. 1009–1020, Apr. 2007.
[31] S. Sharma and B. Singh, "Voltage and frequency control of asynchronous generator for stand-alone wind power generation," *IET Power Electron.*, vol. 4, no. 7, pp. 816–826, Aug. 2011.
[32] G. Abad, J. López, M. Rodríguez, L. Marroyo, and G. Iwanski, *Doubly Fed Induction Machine: Modeling and Control for Wind Energy Generation Applications*. Hoboken, NJ, USA: Wiley\IEEE Press, 2011.
[33] B. Singh and J. Solanki, "A comparison of control algorithms for DSTATCOM," *IEEE Trans. Ind. Elect.*, vol. 56, no. 7, pp. 2738–2745, Jul. 2009.
[34] B. K. Bose, *Modern Power Electronics and AC Drives*, 4th ed. Englewood Cliffs, NJ, USA: Prentice-Hall, 2007, ch. 5.
[35] *IEEE Recommended Practices and Requirements for Harmonic Control in Electrical Power Systems*, IEEE Standard 519, 1992.

N. K. Swami Naidu (M'14) received the B.Tech. degree in electrical and electronics engineering from Jawaharlal Nehru Technological University (JNTU), Hyderabad, India, in 2007; the M.Tech. degree in power electronics and drives from the National Institute of Technology, Kurukshetra, India, in 2009; and the Ph.D. degree from the Electrical Engineering Department, Indian Institute of Technology Delhi, New Delhi, India, in 2015.

He is currently working as a Research Fellow with Nanyang Technological University, Singapore. His research interests include power electronics, wind energy conversion systems, power quality, and microgrid-based power systems.

Bhim Singh (SM'99–F'10) received the B.E. degree in electrical engineering from the University of Roorkee, Roorkee, India, in 1977, and the M.Tech. degree in power apparatus and systems and the Ph.D. degree from the Electrical Engineering Department, Indian Institute of Technology Delhi (IITD), New Delhi, India, in 1979 and 1983, respectively.

In 1983, he joined the Department of Electrical Engineering, University of Roorkee, Roorkee, India, as a Lecturer, and became a Reader there in 1988. In December 1990, he joined the Department of Electrical Engineering, IITD, as an Assistant Professor, where he became an Associate Professor in 1994 and a Professor in 1997, and where he was ABB Chair Professor from September 2007 to September 2012. Since October 2012, he has been a Central Electricity Authority (CEA) Chair Professor with IIT Delhi, New Delhi, India. His research interests include power electronics, electrical machines, electric drives, power quality, renewable energy, flexible ac transmission systems, high-voltage dc transmission systems.

Prof. Singh is a Fellow of the Indian National Science Academy (NA); the Indian National Academy of Engineering (NAE); the National Academy of Science, India (NASc); the Indian Academy of Sciences, India (ASc); the World Academy of Sciences; the Institute of Engineering and Technology; Institution of Engineers (India); and the Institution of Electronics and Telecommunication Engineers (IETE), and a Life Member of the Indian Society for Technical Education (ISTE), the System Society of India, and the National Institution of Quality and Reliability. He has been the General Chair of the IEEE International Conference on Power Electronics, Drives, and Energy Systems (PEDES'2006), and the Co-General Chair of PEDES'2010 held in New Delhi. He has guided 45 Ph.D. dissertations, 139 M.E./M.Tech. theses, and 60 B.E./B.Tech. projects. He has been granted one U.S. patent and filed 12 Indian patents. He has executed more than 60 sponsored and consultancy projects. He was the recipient of the Khosla Research Prize of the University of Roorkee in the year 1991, the JC Bose and Bimal K. Bose Awards of the IETE for his contribution in the field of power electronics, the Maharashtra State National Award of ISTE in recognition of his outstanding research work in the area of power quality, the Power and Energy soceity Delhi Chapter Outstanding Engineer Award in 2006, and the Khosla National Research Award of Indian Institute of Technology Roorkee, in 2013.